

# Time-lapse Diffraction Tomography for Trigonal Meshes with Temporal Data Integration Applied to CO<sub>2</sub> Sequestration Monitoring

Eduardo T. F. Santos<sup>\*1</sup> and Jerry M. Harris, Stanford University.

## Summary

Time-lapse imaging has been successfully applied by oil industry for reservoir monitoring along the years. Another relevant application using similar theoretical background although with different purposes, is to monitor CO<sub>2</sub> sequestration to detect possible leaks that may cause environmental impact. We propose to reduce the number of parameters and consequently to simplify the update surveys by two complementary key concepts: (1) keeping relevant information from previous surveys to be updated by a smaller new survey; (2) using adaptive trigonal mesh that is finer at predicted time-varying regions and coarser otherwise. To achieve our goals, we proposed an approach to integrate data from previous surveys joint with an adaptive trigonal mesh framework applied to diffraction tomography. We used these concepts to develop an inversion algorithm for CO<sub>2</sub> sequestration monitoring, which successfully imaged a synthetic model using VSP geometry.

## Introduction

Time-lapse imaging has been successfully applied for monitoring EOR by oil and gas industry (Lumley, 2001). CO<sub>2</sub> sequestration monitoring became another important application (Davis et al., 2003) (Lazaratos and Marion, 1997). A common approach to monitor subsurface properties is to perform conventional surveys repeated along time. Since the expected image change is due to CO<sub>2</sub> effects on velocity field, the conventional approach tries to estimate more parameters than needed because geological features remain the same along monitoring time. It may also generate image artifacts when computing differences between surveys due to different successive estimations of same geological structures (Rickett and Lumley, 2001). In order to minimize such undesirable effects, we propose a temporal integration technique combined with reduction in the number of parameters to be estimated. The temporal integration is accomplished by joint inversion of previous surveys, damping its influence into current model estimation since newer surveys are more strongly related with current subsurface image. Reduction in the number of parameters was achieved by a framework for trigonal mesh mapping. The adaptive trigonal mesh (Ajo-Franklin, 2006) used to perform inversion has as one of its advantages a higher level of detail close to the contours of injected CO<sub>2</sub>. Another advantage of adaptive mesh methods is the implicit spatial regularization that occurs due to the use of coarser meshes at slow-varying regions. Thus, we reduced the number of parameters to be estimated using adaptive

trigonal adaptive mesh, temporal integration and spatial regularization (Tikhonov, 1977), allowing optimized smaller update surveys. These smaller and less expensive update surveys may be performed by a permanent acquisition system, allowing *quasi* real-time monitoring.

## Trigonal Meshes

We propose the use of trigonal meshes for diffraction tomography in order to reduce the number of parameters to be estimated. However, we also want to keep the simple formulation of tomographic matrix and regularization for conventional regular grids. Thus, we derived a different formulation for the use of trigonal meshes that allows mapping between triangle vertexes and regular grid. This approach can be used as a general framework to solve linear inverse problems for different areas using triangles instead of cells as basic elements, with minimal impact into original problem formulation. The key concept is to describe each cell of a regular grid as a linear combination of control nodes values at triangle vertexes, considering the respective triangle that covers each region of regular grid. Thus, a linear operator  $T$  may be explicitly defined to map any regular grid into control nodes of a trigonal mesh. This approach has also as advantage the possibility of use of its inverse mapping  $T^{-1}$  to find a regular grid representation from a trigonal representation, which is useful to display the resulting image of tomographic inversion. The algorithm that computes matrix  $T$  has the following steps for each triangle of mesh:

- 1) Identify its three vertexes to compute three respective vertex weights based on relative position of interior cells of this triangle;
- 2) Compute three weights for each cell of regular grid within current triangle using barycentric coordinates interpolation;
- 3) Store these weights into a matrix  $T$  that maps each cell value as a linear combination of control nodes triangle vertexes.

The interpolation using barycentric coordinates is based on the areas of three imaginary triangles formed by lines between triangle vertexes and an interior point (Bottema, 1982). These three areas are used as a measurement of influence of each control node vertex onto a point belonging to a triangular mesh element, resulting in three respective weights for each discretized interior point. Considering  $v_1$ ,  $v_2$  and  $v_3$  as the control values at respective positions  $\mathbf{r}_1$ ,  $\mathbf{r}_2$  and  $\mathbf{r}_3$  corresponding to vertexes of each triangle, the weights for each interior point at position  $\mathbf{r}$  using barycentric interpolation are given by the following expressions:

<sup>1</sup> licensed for postdoctoral scholarship by Federal Center of Technological Education of Bahia (CEFET-BA), Brazil.

## Time-lapse Diffraction Tomography Applied to CO<sub>2</sub> Sequestration Monitoring

$$w_1(\mathbf{r}) = \frac{(\mathbf{r}-\mathbf{r}_2) \times (\mathbf{r}_3-\mathbf{r}_2) \cdot \mathbf{e}_3}{(\mathbf{r}_1-\mathbf{r}_2) \times (\mathbf{r}_3-\mathbf{r}_2) \cdot \mathbf{e}_3},$$

$$w_2(\mathbf{r}) = \frac{(\mathbf{r}-\mathbf{r}_1) \times (\mathbf{r}_3-\mathbf{r}_1) \cdot \mathbf{e}_3}{(\mathbf{r}_2-\mathbf{r}_1) \times (\mathbf{r}_3-\mathbf{r}_1) \cdot \mathbf{e}_3},$$

$$w_3(\mathbf{r}) = \frac{(\mathbf{r}-\mathbf{r}_1) \times (\mathbf{r}_2-\mathbf{r}_1) \cdot \mathbf{e}_3}{(\mathbf{r}_3-\mathbf{r}_1) \times (\mathbf{r}_2-\mathbf{r}_1) \cdot \mathbf{e}_3},$$

where  $\mathbf{e}_3$  is the unitary vector  $(0,0,1)$ . This leads to the following expression that maps nodes control values from trigonal mesh into a regular grid cell value  $o(\mathbf{r})$  for each triangle:

$$o(\mathbf{r}) = \sum_{i=1}^3 w_i(\mathbf{r}) v_i(\mathbf{r}).$$

The matrix  $T$  performs this mapping for each cell of regular grid using respective triangles that covers its different regions. Thus, nodes control values at triangle vertexes are mapped into a regular grid using the forward mapping expression  $\mathbf{o} = T\mathbf{v}$ , and the inverse mapping from regular grid into control nodes values of trigonal mesh is given by  $\mathbf{v} = T^{-1}\mathbf{o}$ . This allows a straightforward modification to convert a regular grid method into a trigonal mesh method. From a simple regular grid formulation for linear problems  $\mathbf{p} = W\mathbf{o}$ , where  $\mathbf{p}$  is the data vector and  $\mathbf{o}$  is the parameter vector, one may use the expression for trigonal meshes  $\mathbf{p} = WT\mathbf{v}$ . For linear inverse problems, this expression may be applied to estimate trigonal mesh control node values from data vector:

$$\mathbf{v} = (WT)^+ \mathbf{p},$$

where the superscripted plus symbol means pseudo-inverse (Penrose, 1955) computed using SVD. An equivalent regularized system may also be obtained:

$$\begin{bmatrix} W \\ D \end{bmatrix} T\mathbf{v} = \begin{bmatrix} \mathbf{p} \\ \mathbf{0} \end{bmatrix},$$

where  $D$  is a numerical derivative matrix (Santos, 2006). After parameter estimation, the resulting trigonal mesh control values can be easily displayed as a regular grid using forward mapping of linear operator  $T$ , as described earlier.

### Diffraction Tomography

This section presents the underlying theory of diffraction tomography (Devaney, 1984) (Harris, 1987) (Wu, 1987). The scalar wave equation is given by

$$\nabla^2 U(\mathbf{r}, t) = \frac{1}{c^2(\mathbf{r})} \frac{\partial^2 U(\mathbf{r}, t)}{\partial t^2},$$

where  $U(\mathbf{r}, t)$  is the solution (displacement or pressure) and  $c(\mathbf{r})$  is the velocity of the sound in the medium.

Considering that the solution can be written as  $U(\mathbf{r}, \omega, t) = e^{-i\omega t} P(\mathbf{r}, \omega)$ , which represents a harmonic dependence with time, we obtain the Helmholtz equation:  $[\nabla^2 + k^2]P(\mathbf{r}, \omega) = 0$ , where the 2-D wavenumber is given by  $k = k(\mathbf{r}, \omega) = \sqrt{k_x^2 + k_y^2}$ . The conditions for the imaging are that the medium is acoustic and 2-D, the propagation of the incident field is within an limited area  $A(\mathbf{r}')$ , and the background has constant velocity  $c_0$ . The object function, defined as

$$O(\mathbf{r}) = 1 - \frac{c_0^2}{c^2(\mathbf{r})},$$

represents the perturbation of the velocity in each point in relation to  $c_0$ . Redefining the wavenumber as function of

$O(\mathbf{r})$ , we have that  $k^2(\mathbf{r}) = k_0^2 - k_0^2 O(\mathbf{r})$ , and substituting it in the Helmholtz equation, we obtain

$$[\nabla^2 + k^2]P_{SCAT} = k_0^2 O(\mathbf{r})[P_0 + P_{SCAT}],$$

where  $P_0$  is the incident field and  $P_{SCAT}$  is the scattered field. The last differential equation has the following integral solution:

$$P_{SCAT}(\mathbf{r}) = -k_0^2 \int_{A(\mathbf{r}')} O(\mathbf{r}') G(\mathbf{r} | \mathbf{r}') [P_0(\mathbf{r}') + P_{SCAT}(\mathbf{r}')] d\mathbf{r}'.$$

The above equation is nonlinear and the linearization was achieved using the first order Born approximation, which is only valid for the weak scattering of the incident field. The total field is  $P_T(\mathbf{r}) = P_0(\mathbf{r}) + P_{SCAT}(\mathbf{r})$  so that we have

$P_T(\mathbf{r}) \approx P_0(\mathbf{r})$ . Thus we obtain a linear relation between the object function and the scattered field:

$$P_{SCAT}(\mathbf{r}) = -k_0^2 \int_{A(\mathbf{r}')} O(\mathbf{r}') G(\mathbf{r} | \mathbf{r}') P_0(\mathbf{r}') d\mathbf{r}'.$$

We represent the incident field by a source at  $\mathbf{r}_S$  through the Green's function  $P_0(\mathbf{r}') = G(\mathbf{r}' | \mathbf{r}_S)$ , and the scattered field in  $A(\mathbf{r})$  is registered by a receptor at  $\mathbf{r}_G$ :

$$P_{SCAT}(\mathbf{r}_S, \mathbf{r}_G) = -k_0^2 \int_{A(\mathbf{r}')} O(\mathbf{r}') G(\mathbf{r}' | \mathbf{r}_S) G(\mathbf{r}_G | \mathbf{r}') d\mathbf{r}'$$

The discretization of the above relation leads to the linear system  $\mathbf{p} = W\mathbf{o}$ , which has to be inverted in order to recover  $O(\mathbf{r})$  (Rocha Filho, 1997). In this work the inversion was done using SVD. The scattered field computed from the synthetic model was performed using first order Born approximation as well.

### Temporal Data Integration

Time-lapse imaging conventionally requires inversion of different independent data sets for later comparison or

## Time-lapse Diffraction Tomography Applied to CO<sub>2</sub> Sequestration Monitoring

image subtraction analysis to identify changes. This straightforward approach repetitively estimate fixed geology structures, ignoring the similarities between successive images that could be useful during inversion. A smarter approach uses a temporal derivative operator to integrate data along time using previous surveys information combined with update surveys (Ajo-Franklin, 2005). It requires solving an integrated linear system that contains previous surveys equations and temporal derivative equations minimization. We adopted a different approach that integrates previous surveys information but uses a scalar factor to damp the influence of each previous survey into the latest survey information available:

$$\begin{bmatrix} W_k \\ \alpha_{k-1}W_{k-1} \\ \vdots \\ \alpha_{k-ns+1}W_{k-ns+1} \end{bmatrix} \mathbf{0} = \begin{bmatrix} \mathbf{p}_k \\ \alpha_{k-1}\mathbf{p}_{k-1} \\ \vdots \\ \alpha_{k-ns+1}\mathbf{p}_{k-ns+1} \end{bmatrix},$$

where index  $k$  represents the newest survey,  $ns$  is the number of available surveys and  $\alpha_{k-i}$  is a normalized scalar proportional to the influence of earlier survey  $k-i$  into current inversion, being smaller for older surveys. Since relevant information from previous surveys is included in this equivalent system, a new smaller and less expensive survey may be performed to update subsurface image. This procedure can be repeated for newer surveys and keeps relevant information from previous ones, increasing the number of rows by the number of newer survey equations but keeping fixed the number of columns of equivalent linear system, which may not occur when using temporal derivative operator approaches. Thus, this approach joins computational performance for integrated inversion, previous surveys information and optimized smaller update surveys.

### Numerical Simulation

We considered true models with  $50 \times 50 = 2,500$  cells, which are presented for successive time-lapses of CO<sub>2</sub> flood in Figures 1a, 2a, 3a, 4a and 5a. All figures show distances in meters and velocities in m/s. It was adopted VSP geometry, where sources are located at the top of true model and receivers are located at left vertical border, both evenly spaced. The figures show only the velocity field difference when compared with background medium ( $\sim 4,000$  m/s). There is a negative velocity contrast (2%) caused by CO<sub>2</sub> injection. This model shows that injected CO<sub>2</sub> at bottom level escaped through a leak due to a fault, forming an upper plume, an important situation to be detected. A baseline survey is performed using 28 sources and 28 receivers for true model shown in Figure 1a. A trigonal adaptive mesh (Figure 1b) is generated based on velocity gradient from a priori information, leading to the inversion result shown in Figure 1c. A regular grid would

provide good results for this base survey as well, since a reasonable number of sources and receivers was employed. *A priori* information to generate adaptive meshes may come from reservoir flow simulation prediction or from previous surveys. The meshes were generated using function calls to a Matlab toolbox called Distmesh (Persson, 2004). The proposed adaptive mesh inversion reduces the number of parameters but still keeps robustness, since triangles at slow-varying velocity fields regions are coarser but still useful to perform good imaging even with low quality *a priori* information. Since the previous surveys information is integrated into inversion, the successive update surveys use a smaller and consequently less expensive survey with half of the data measurements when compared with baseline survey. In our example, we adopted a constant scalar for the immediately previous survey  $\alpha = 0.3$  and adopted respectively  $\alpha^2$ ,  $\alpha^3$  and so on when other earlier surveys were available and evenly sampled along time. We applied spatial regularization for order 2 and  $\lambda = 0.02$  for all inversions. A naive regular grid inversion for such image resolution would require 50 sources and 50 receivers for each time-lapse inversion, which means it would require three times more data measurements than we used. Successive update images are shown in Figures 2-5, each set displaying true model (a), adaptive mesh (b) and trigonal mesh inversion (c).

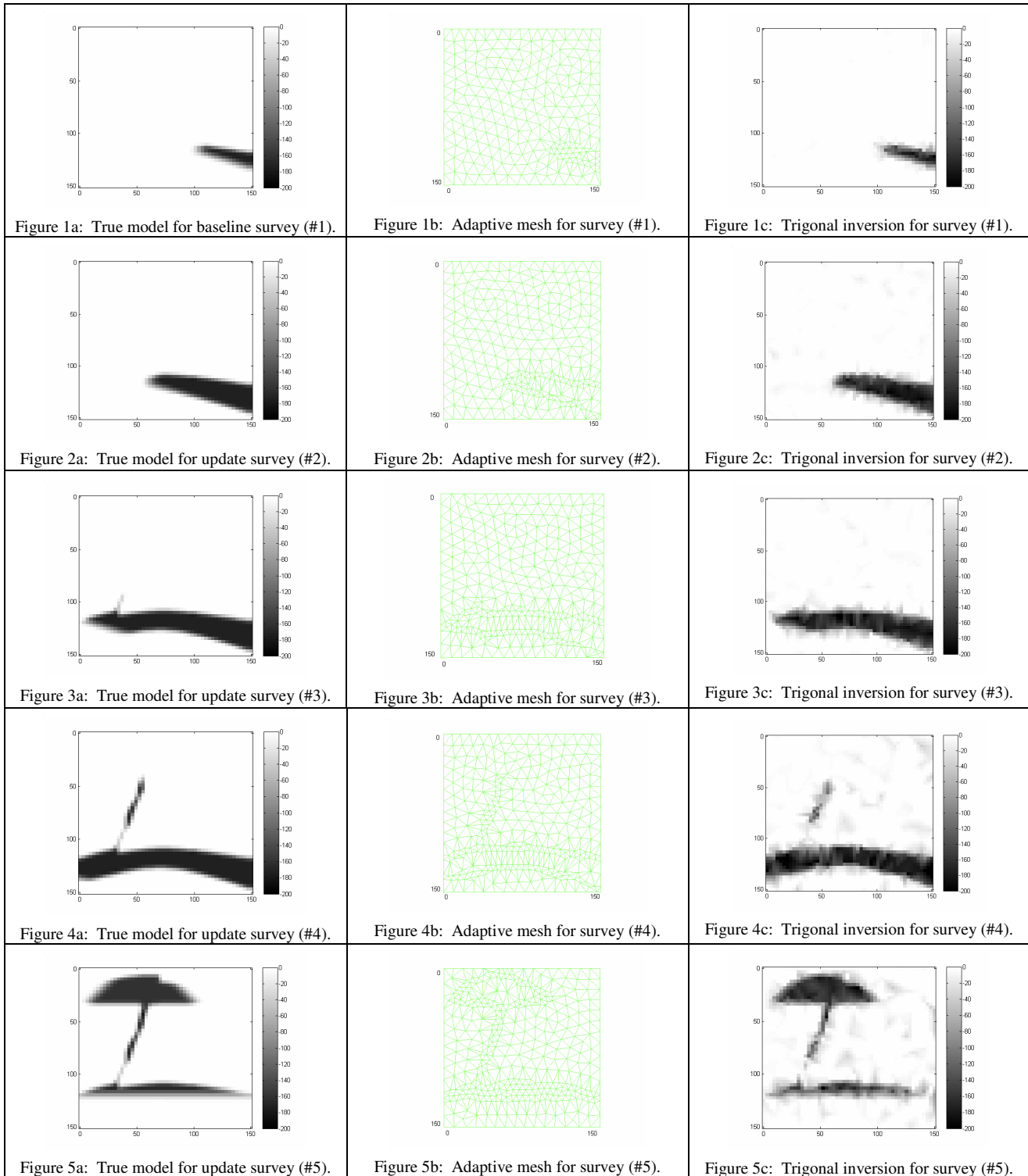
### Conclusions

We proposed an adaptive trigonal mesh mapping with temporal integration for inversion problems and successfully applied it to time-lapse diffraction tomography. The use of adaptive meshes strongly reduced the number of parameters to be estimated. This reduction was reinforced by temporal integration of previous survey to achieve current subsurface image. Thus, problems that were originally underdetermined can be reformulated as overdetermined without the drastic decrease of resolution required for regular grids under similar circumstances. We showed through a synthetic model inversion how trigonal meshes and temporal integration of previous surveys reduce the number of parameters, successfully detecting the CO<sub>2</sub> target.

### Acknowledgements

The authors would like to acknowledge Jaime Urban for original CO<sub>2</sub> model adapted in this work. We also would like to acknowledge the following institutions for research support: Stanford University (the Global Climate and Energy Project, the Smart Fields industrial affiliates, and the Center for Computational Earth and Environmental Science) and Federal Center of Technological Education of Bahia (CEFET-BA).

## Time-lapse Diffraction Tomography Applied to CO<sub>2</sub> Sequestration Monitoring



## EDITED REFERENCES

Note: This reference list is a copy-edited version of the reference list submitted by the author. Reference lists for the 2007 SEG Technical Program Expanded Abstracts have been copy edited so that references provided with the online metadata for each paper will achieve a high degree of linking to cited sources that appear on the Web.

## REFERENCES

- Ajo-Franklin, J. B., J. A. Urban, and J. M. Harris, 2005, Temporal integration of seismic traveltimes tomography: 75th Annual International Meeting, SEG, Expanded Abstracts, 2468–2471.
- , 2006, Using resolution-constrained adaptive meshes for traveltimes tomography: *Journal of Seismic Exploration*, 14, 371–392.
- Bottema, O., 1982, On the area of a triangle in barycentric coordinates: *Crux Mathematicorum*, 8, 228–231.
- Davis, T., M. R. B. Terrel, R. Cardona, R. Kendall, and R. Winarsky, 2003, Multicomponent seismic characterization and monitoring of the CO<sub>2</sub> flood at Weyburn Field, Saskatchewan: *The Leading Edge*, 22, 696–697.
- Devaney, A. J., 1984, Geophysical diffraction tomography: *IEEE Transactions on Geoscience and Remote Sensing*, 22, 3–13.
- Harris, J. M., 1987, Diffraction tomography with discrete arrays of sources and receivers: *IEEE Transactions on Geoscience and Remote Sensing*, GE-25, 448–455.
- Lazaratos, S., and B. Marion, 1997, Crosswell seismic imaging of reservoir changes caused by CO<sub>2</sub> injection: *The Leading Edge*, 16, 1300–1306.
- Lumley, D., 2001, Time-lapse seismic reservoir monitoring: *Geophysics*, 66, 50–53.
- Penrose, R., 1955, A generalized inverse for matrices: *Proceedings of the Cambridge Philosophical Society*, 51, 406–413.
- Persson, P. O., and G. Strang, 2004, A simple mesh generator in MATLAB: *SIAM Review*, 46, 329–345.
- Rickett, J., and D. Lumley, 2001, Cross-equalization data processing for time-lapse seismic reservoir monitoring: A case study from the Gulf of Mexico: *Geophysics*, 66, 1015–1025.
- Rocha Filho, A. A., 1997, *Formulação matricial multifrequência e inversão integrada* (in Portuguese): M.S. dissertation, Federal University of Bahia.
- Santos, E. T. F., 2006, *Inversão tomográfica sísmica anisotrópica com regularização ótima* (in Portuguese): D.Sc. thesis, Federal University of Bahia.
- Tikhonov, A. N., and V. Y. Arsenin, 1977, *Solution of ill-posed problems*: Wiley and Sons.
- Wu, R. S., and M. N. Toksöz, 1987, Diffraction tomography and multisource holography applied to seismic imaging: *Geophysics*, 52, 11–25.